Ph.D. DISSERTATION

Electrical detection of Troponin i based on aptamer as a probe molecule

(압타머 프로브 물질을 기반으로 한 트로포닌 i 의 전기적 검출에 관한 연구)

By

Hoseok Lee

August 2018

SCHOOL OF ELECTRICAL ENGINEERING AND COMPUTER SCIENCE
COLLEGE OF ENGINEERING
SEOUL NATIONAL UNIVERSITY

Electrical detection of Troponin i based on aptamer as a probe molecule

(압타머 프로브 물질을 기반으로한 트로포닌 I 의 전기적 검출에 관한 연구)

指導敎授 朴 榮 俊

이 論文을 工學博士 學位論文으로 提出함

2018 年 8 月

서울大學校 大學院

電氣–컴퓨터 工學部

李 昊 錫

林 載 興의 工學博士 學位論文을 認准함

2018 年 8 月

委 員 長	이 종 호	(印)
副委員長	전 국 진	(印)
委 員	박 영 준	(印)
委 員	정 준 호	(印)
委 員	신 동 식	(印)

Electrical detection of Troponin i based on aptamer as a probe molecule

by

Hoseok Lee

Submitted to the School of Electrical Engineering and Computer Science
in partial fulfillment of the requirements for the degree of
Doctor of Philosophy in Electrical Engineering
at
SEOUL NATIONAL UNIVERSITY
August 2018

Committee in Charge:

Jong Ho Lee, Chairman
Kukjin Chun, Vice-Chairman
Young June Park
Junho Chung
Dong-Sik Shin

Abstract

Rapid detection of cardiac biomarkers is an important factor for the diagnosis of acute myocardial infarction (AMI). The cardiac troponin I (cTnI) is at present a promising biomarker for diagnosis of AMI.

In this dissertation, we demonstrate an effect of electrical control approach for a carbon nanotube network (CNN) based biosensor platform to detect the cTnI.

The carbon nanotube (CNT) channel between the concentric electrodes is formed by the dip-coating method. The CNN channel region is decorated with gold nanoparticels (GNPs), which act as attaching sites of the probe molecules.

The contribution of this dissertation can be summarized in three approaches.

First, we employ aptamer as the probe molecule in this research since it has high affinity and specificity to cTnI for biosensing application. The aptamer is immobilized on the AuNP by forming the gold-thiol chemical bonds. The method of AC electrothermal flow (ACEF) was first introduced to our biosensor platform improve the affinity between the probe and the target molecules.

Second, the pulse measurement was used as the method of electrical detection and the current change was analyzed in the transient state. To

enhance the performance of the sensor platform, the method of integration current was proposed in this study.

Third, in order to demonstrate the applicability of the technology for point of care testing (POCT), we conducted validation studies with the biosensor platform to detect cTnI in the human serum conditions. As a result, the detection limit of the sensor platform is a low as 4.5pg/ml in a human serum added solution (cut off value of cTnI: 45pg/ml~1pM).

Keywords: Carbon nanotube, gold nanoparticle, aptamer, troponin I protein sensor, AC electro thermal flow(ACEF), Acute myocardial infarction (AMI)

Student Number: 2012-20848

Contents

List of Tables

List of Figures

Chapter 1

Introduction

1.1 Motivation

The World Health Organization (W.H.O.) lists cardiovascular diseases (CVDs) as the leading cause of death globally [1]. Among CVDs, acute myocardial infarction (AMI) is one of the most life-threatening diseases due to diminished flow of blood to the heart. The early diagnosis of AMI and appropriate immediate treatment is important to minimize myocardial injury. The cardiac biomarkers are the indicators, which have been mainly used in the detection of AMI. The most commonly used biomarkers are creatine kinase-MB, myoglobin, cardiac troponin T (cTnT), and cardiac troponin I (cTnI) [2]. Currently, the use of cardiac troponin (cTn) is the reference standard in the AMI diagnostics [3]. Most emergency departments do not meet the suggested turnaround time for the cTn diagnostic results within 60minutes [4].

In order to have reliable diagnostic tools for the rapid detection and identification of biological agents, new methods should be developed that will

permit label-free and real time measurement of simultaneous interactions. Biosensing devices, fabricated by means of nanotechnologies, are powerful devices that can fulfill these requirements and have the added draw of being portable, making “point-of-care (POC)” analysis possible [5].

In this thesis, possible ways to overcome the general issues posed by the FET-based electrical biosensor platform are proposed and experimentally verified for practical applications. The contribution of this paper is to improve the affinity between the probe aptamer and the target troponin through the electrical measurement, and to demonstrate the applicability of point of care testing (POCT) technology, we conducted a validation study using the biosensor platform in the human serum conditions.

1.2 AC electrokinetic techniques

In most biosensors, the recognition event such as the antigen – antibody reaction or the oligonucleotide hybridization occurs between the target molecules in the sample solution and the probe molecules adsorbed on sensor surface. It can be described by the first-order Langmuir kinetics according to the following equation,

$$\frac{\partial B}{\partial t} = k_{\mathrm{on}} c_s (P - B) - k_{\mathrm{off}} B,$$

where P is the surface concentration of the probe molecules, B is the surface concentration of the probe molecules bound with target molecules, c_s is the concentration of target molecules at the sensor surface, k_{on} is the association rate, and k_{off} is the dissociation rate.

In order for the affinity-based biosensors to be used for fast POCT devices, the detection time should be improved especially in the solution with low target concentration. The detection time is limited by the slow probe-target binding process [6], [7]. As the target molecules are captured and depleted at the sensor surface, the whole binding process is limited by the transport of the target molecules toward the sensor surface by diffusion as

$$\frac{\partial c}{\partial t} = D\nabla^2 c,$$

where c is the concentration of target molecules, and D is the diffusion coefficient of target molecules.

To improve the situation, it has been introduced that additional force should be exerted to the target molecules to induce fast flux toward the sensor surface. Recently, AC electrokinetic forces have emerged as simple particle manipulating methods that can be exploited in various microscale applications [7], [8]. The non-uniform electric field generated by AC biasing to the microelectrode structure can give rise to various types of phenomena, which

are AC electrothermal flow, AC electroosmosis, and dielectrophoresis. Among them, AC electrothermal flow (ACEF) is suitable for biosensors since it can effectively operate in highly conductive biological media (~ 1 S/m).

In this thesis, we present an effective affinity-based sensing strategy which can significantly enhance sensing speed by combining the structural advantages of carbon nanotube network (CNN) based electrical biosensor platform and the microstirring effect of ACEF. Our biosensor platform consists of two concentric-shaped electrodes; one is a small island electrode and the other is a large-area enclosing electrode. Therefore, by applying AC bias between these two electrodes, we can easily induce the ACEF and affect the transport process as predicted by,

$$\frac{\partial c}{\partial t} + \vec{v} \cdot \nabla c = D\nabla^2 c,$$

where $\vec{v}$ is the velocity of the fluid.

1.3 Outline of the Dissertation

This dissertation is organized as follows.

In chapter 2, CNT based biosensor device for protein sensing is described. The basic fabrication process of the sensor device, the CNT channel formation, and deposition of the gold nanoparticle by thermal evaporation are described.

In chapter 3, The theoretical background and physical principles of AC electrokinetics are listed.

In chapter 4, the electrical sensor performance is explained by detecting cardiac troponin I (cTnI), which is a specific cardiac biomarker for the diagnosis of acute myocardial infarction (AMI). Also, it will be shown that a LOD of as low as ~1pM concentration can be achieved, in the detection of cTnI in the human serum conditions. (cut off value of cTnI: 45pg/ml~1pM).

In chapter 5, the electrical methods to enhance the sensor performance are explained. The detail procedure and their experimental results are shown.

In chapter 6, the conclusion and suggestions for the further works are given.

Chapter 2

Experimental sensor platform

2.1 Introduction

In this chapter, the fabrication process of the device platform and basic electrical properties will be described [10]–[15].

The structure of the device in this work adopted asymmetric and concentric structure where the small island electrode is surrounded by the large enclosing electrode. The concentric two-electrode structure shows the asymmetric I-V characteristics in electrolyte conditions known as a “self-gating effect” [13].

The carbon nanotube (CNN) is formed on the channel area between concentric electrodes by a dip coating method.

The gold nanoparticles (GNPs), which act as attaching sites of the probe molecules, are deposited on the CNN channel region by a thermal evaporation process.

In addition, we have described the immobilization of aptamers in GNPs on CNTs.

2.2 Preparation of the Sensor

The sensor platforms were fabricated at the Inter-University Semiconductor Research Center(ISRC) of Seoul National University, using a conventional one-metal process, which consisted of Ti/Au as a metal electrode. After deposition of the 50nm thick Ti on top of the thermally grown SiO_2 with a thickness of 1um, a 15um channel length is formed by the liftoff process of Au layer with a thickness of 200nm.

For the channel formation between the two electrodes, we used a dip-coating method. The prepared swCNTs (ASP-100F produced by Il-jin Nanotech, Korea) were dispersed in 1,2-dichlorobenzene solution with a concentration of 0.01 mg/mL, and then an ultra-sonication process is performed for 30min. The fabricated chip was immersed in a swCNT colloidal solution and pulled out at a constant withdrawal velocity of 3mm/min. During the dip-coating, swCNT bundle was deposited on the surface of the oxide surface in the form of a network [16]. The diameter of the nanotubes, measured using an atomic force microscope, appears to be less than 1.5nm, indicating that they are mostly single-walled.

The next step is the Au deposition process on the swCNT to provide the attaching place for the probe molecules and to enhance the attachment of the swCNT to the Au electrode during the overall swCNT sensor device

integration [17]. Deposition of gold nano particle(GNP) on the swCNT network was performed by thermal evaporation method. The detail processing conditions to decorate the nanoparticle are as follows. The pressure in the evaporation chamber is pumped down to 2.0×10^{-2} Torr by a rotary pump, and followd by pumping down to 9.0×10^{-6} Torr by a turbomolecular pump. After the pressure is stabilized, a voltage is applied across the tungsten boat filament containing the metal sources to raise temperature. The deposition rate and thickness was monitored using a quartz crystal microbalnce(QCM) [18]. In this work, the thickness of all the metal nanoparticle is adjusted to be 1nm at 1 Å /sec of deposition rate in 10 seconds. The diameter of Au on the swCNT was about 10nm. The array of the concentric electrode structure was formed as shown in the figure 2-1.

2.3 Feature of the concentric electrode structure [13]

The two electrodes, one electrode is enclosed by the other electrode, have the asymmetric shape. While the electrolyte as the gate is floated electrically, however, it is capacitively coupled with the island electrode (drain) and enclosing electrode (source). Due to the much larger area of enclosing electrode than that of island electrode, the electrostatic potential of the

electrolyte solution is determined by the potential applied to enclosing electrode without any reference electrode. This concentric electrode structure has great advantage in implementing sensor array and provides an interesting feature called the “self-gating effect”. The figure. 2-2 (a) and (b) shows the schematics diagram of the concentric structure and its equivalent circuit. The figure. 2-2 (c) shows the I-V characteristics of a representative bare CNN device in which the drain voltage is swept from -0.5V~ to +0.5V.

2.4 Immobilization of probe molecule aptamer

For the application of this sensor platform to the protein sensing, the aptamer immobilization is performed on the channel of CNN decorated with GNP. The sensor platform for the detection of cTnI, which is known as the biomarker related with the AMI, were constructed.

Tro4 and Tro6 aptamers exhibit bivalent binding capacity toward cTnI, indicating that each aptamer is bound to different K_d value (table 2-1).

The binding affinity of aptamer candidates was evaluated as K_d values, which were measured by SPR [19]. The Tro6 aptamer samples were purchased from Bioneer, Inc. (Korea).

To monitor whether Tro6 aptamer molecules are well anchored on the GNPs,

the real-time current flow through the CNN was monitored during the immobilization process (figure 2-4). Constant voltage (0.1V) was applied to the drain (island electrode) and the current was measured. To compare with the normal PBS solution which does not contain a Tro6 aptamer, the normalized current is analyzed by dividing the real-time current by the initial current. As we can see from the figure 2-4, the current change in the Tro6 aptamer solution was remarkable compared with the normal PBS solution. This difference can be attributed to the modulation of the work function of GNPs induced by the formation of gold thiol chemical bonds [12].

Aptamer	**Sequence**	**K_d value (cTnI)**
Tro1	5'-TCACACCCTCCCTCCCACTACCGCATACACTTTCTGATT-3'	3.41nM
Tro2	5'-CCCGACCACGTCCCTGCCCTTTCCTAACCTGTTTGTTGAT-3'	1.13nM
Tro3	5'-ATGCGTTGAACCCTCCTGACCGTTTATCACATACTCCAGA-3'	1.14nM
Tro4	5'-CGTGCAGTACGCCAACCTTTCTCATGCGCTGCCCCTCTTA-3'	270pM
Tro5	5'-CAACTGTAATGTACCCTCCTCGATCACGCACCACTTGCAT-3'	3.25nM
Tro6	5'-CGCATGCCAAACGTTGCCTCATAGTTCCCTCCCCGTGTCC-3'	317pM

Table 2-1 Several types of aptamers that respond to cTnI and their sequences and dissociation constants [19].

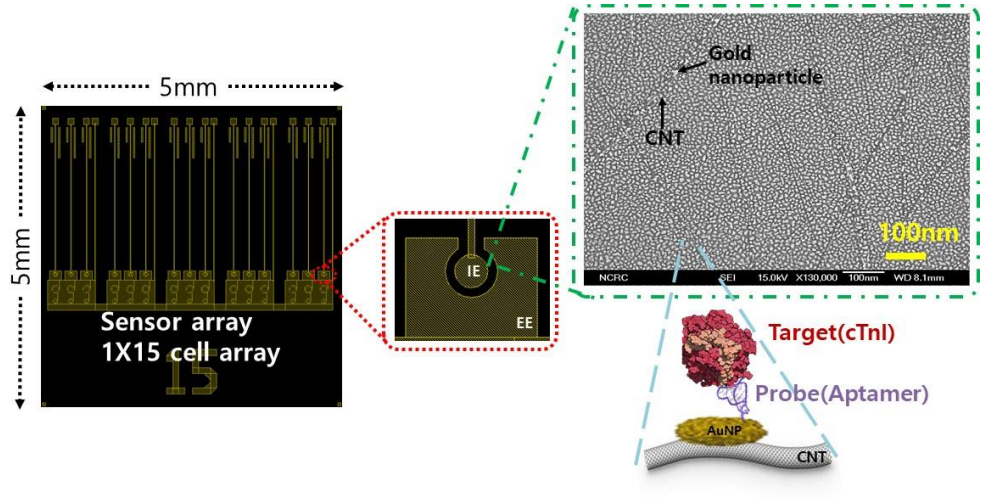

Figure 2-1 Schematic representation of the device structure. Each cell consists of the concentric structure where the small island electrode is surrounded by the large enclosing electrode. The channel region consists of the carbon nanotube network (CNN) as the electrical channel and gold nanoparticles(GNPs) which act as attaching sites of the probe molecules.

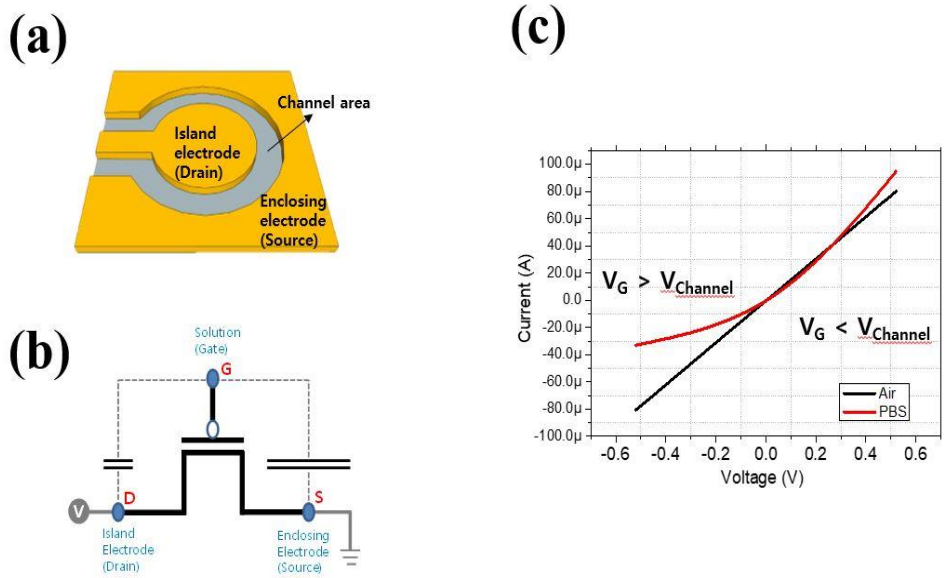

Figure 2-2 (a) The schematics of concentric structure. (b) The equivalent circuit diagram. (c) The current versus voltage characteristics of the test platform. concentric structure gives self-gating effect in the solution [13].

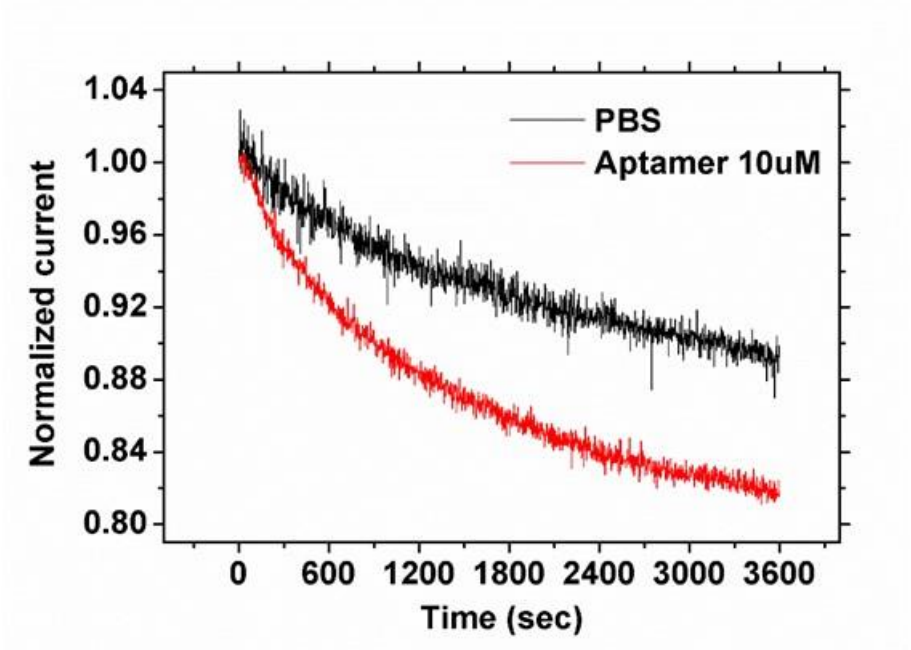

Figure 2-3 Real-time monitoring of current during the Tro6 aptamer immobilization process. Black line show the current change when only the PBS solution is includeed and the red line shows the current change when the solution containing the aptamer is deopped (red-line).

Chapter 3

Effect of AC electrokinetics on the binding events

3.1 Introduction

The development of automated microfluidic system poses great promises for a variety of medical diagnosis applications [20]. Among numerous micro fluidic techniques, the alternating current (AC) electrokinetics is one of the most promising approaches. AC electrokinetics have emerged as simple particle-manipulating methods that can be exploited in various microscale applications [21], [22]. The nonuniform electric field generated on the microelectrode structure by AC biasing can give rise to various types of phenomena such as AC electrothermal flow(ACEF), AC electro-osmosis(ACEO), and dielectrophoresis(DEP). Among them, dielectrophoresis and AC electroosmosis are effective only in low-conductivity fluids. AC electrothermal flow, on the other hand, is effective in fluids that have a wide range of conductivity [23]. Therefore, the ACEF is suitable for biosensors as it can effectively operate in highly conductive biological media(~1S/m).

3.2 AC electrothermal flow(ACEF)

The ACEF results from the ionic conduction current which is driven by a nonuniform electric field. Then, an associated local Joule heating effect occurs and a locally increased temperature profile leads to gradients in the solution permittivity and conductivity. As a result of the combined effect of these gradients and the applied electric field, an electrokinetic force is exerted on the on the fluid so that various species of particles in the sample solution, even small molecules, can be stirred by the induced electrothermal flow.

Our biosensor platform consists of two concentric electrodes: one is a small island electrode(IE) and the other is a large enclosing electrode (EE). By applying AC bias between these two electrodes, we can easily generate a nonuniform electric field in the electrolyte and induce ACEF. The thermally induced flow contributes to the transport process with additional convective terms

$$\frac{\partial c}{\partial t} + \vec{v} \cdot \nabla c = D\nabla^2 c$$

Where $\vec{v}$ is the velocity of the fluid. We used experiments to verify that the ACEF induced using our biosensor platform can assist the transport of the target molecules toward the sensor surface so that the overall binding process

can be accelerated, which leads to enhanced sensor performance.

To obtain an expression for $\vec{v}$, which is the most important parameter to determine the binding event, First, the two-dimensional quasi-static potential field is calculated, according to Laplace's equation,

$$\nabla^2 V = 0$$

The resulting electric field, given by

$$\vec{E} = -\nabla V.$$

Then, the local temperature (T) increased by local Joule heating can be estimated by solving the energy balance equation

$$\rho_m c_p \vec{v} \cdot \nabla T + \rho_m c_p \frac{\partial T}{\partial t} = k\nabla^2 T + \sigma|\vec{E}|^2,$$

where ρ_m is the mass density of the fluid, c_p is the heat capacity of the fluid (at constant pressure), k is the thermal conductivity of the fluid, and σ is the electrical conductivity of the fluid.

Ignoring unsteady effects and convection, and balancing thermal diffusion with Joule heating yields

$$k\nabla^2 T + \sigma|\vec{E}|^2 = 0$$

The temperature gradient generated by Joule heating induces the gradient of permittivity (ε) and conductivity (σ) of the solution [24],

$$\nabla\varepsilon = \left(\frac{\partial\varepsilon}{\partial \mathrm{T}}\right)\nabla \mathrm{T},$$

$$\nabla\sigma = \left(\frac{\partial\sigma}{\partial \mathrm{T}}\right)\nabla \mathrm{T}.$$

In turn, these gradients induce a space charge density (ρ) in the solution, which can be described by Gauss's law and the charge conservation equation

$$\rho = \nabla\cdot\left(\varepsilon\vec{E}\right) = \nabla\varepsilon\cdot\vec{E} + \varepsilon\nabla\cdot\vec{E},$$

$$\frac{\partial\rho}{\partial \mathrm{t}} + \nabla\cdot\left(\sigma\vec{E}\right) = 0.$$

Then, we can estimate the thermally induced body force $\overrightarrow{(F_E)}$, ans expressed in ref [8].

$$\overrightarrow{F_E} = -\frac{1}{2}\left[\left(\frac{\nabla\sigma}{\sigma} - \frac{\nabla\varepsilon}{\varepsilon}\right)\cdot\vec{E}\,\frac{\varepsilon\vec{E}}{1+(\omega\tau)^2} + \frac{1}{2}\left|\vec{E}\right|^2\nabla\varepsilon\right],$$

Where $\tau = \varepsilon/\sigma$ is the charge relaxation time of the solution.

Finally, the electrothermal force is a body force on the fluid. The motion of the fluid can be determined by solving the Stokes' equation for zero Reynolds number fluid flow, such that

$$0 = -\nabla p + \eta\nabla^2\vec{v} + \vec{F}_E,$$

$$\nabla\cdot\vec{v} = 0$$

,where p is the pressure ,η is the viscosity of the fluid and $\vec{v}$ is the fluid velocity.

The electrothermally induced fluid velocity introduces an additional convective term in the transport equation. Compared with a diffusion-limited

case, in which diffusive transport solely supplies target molecules to the sensor surface, and limits the rate of the whole binding process, the target molecules can now be transported toward the sensor surface by both diffusive transport and convective transport. Because the transport rate, which is the limiting factor of the probe-target binding reaction, can be modified by a convection process, the binding rate can also be changed.

3.3 Simulation on the effect of ACEF [25]

Based on previous model equations, we simulated an AC electrothermal effect on our biosensor platform to gain a clearer understanding of the physical principles and to determine the optimal experimental conditions. All simulations were performanced using the finite elecment analysis software, COMSOL Multiphysics version 5.0 (COMSOL Ltd., Stockholm, Sweden). We simulated the binding reaction of the target molecules (cTnI) with the probe molecules (Tro6 aptamer) for 30min using a time-dependenct solver. The geometry used in the simulation is illustrated in the figure 3-1. All the bottom boundaries were set as the binding region. The exact parameter values and boundary conditions used in the simulation are listed in the tabel 3-1. The parameters of the solution region are chosen to reflect the characteristics of the real experimental condition. We used a normal convergence test to determine

that the simulation results were independent of the mesh used.

The figure 3-2 shows the concentration of the target molecules near the sensor surface at various biases after 60 s. As we increased the amplitude of the AC bias voltage, noticeable phenomena were observed. First, the thickness of the depletion zone was significantly reduced, which indicated that the depletion of the target molecules near the sensor surface was suppressed as a result of the continuous supply of the target molecules from the bulk electrolyte. In particular, the degree of suppression of the depletion zone was at a maximum exactly above the CNN region. To clearly understand this phenomenon, we plotted the flow velocity field at 5 V AC bias in figure 3-2(e). Interestingly, a fast vortex (maximum speed$\sim 1.5 \times 10^{-3} m/s$) was formed exactly above the sensor surface. Owing to the microstirring effect of the induced vortex, the target molecules were continuously transported to the CNN region. These results indicate that our concentric array-type platform has an extremely suitable geometry to take advantage of ACEF.

Second, AC biasing led to a significant enhancement of the binding rate compared with that under unbiased conditions. We plotted the dimensionless bound probe molecule (B/Beq), where Beq denotes the surface concentration of the bound probe molecules in equilibrium, as shown in figures 3-3(a) and (b) for the unbiased conditions and 5 V AC biased conditions, respectively.

The binding event between the probe and target molecules occurred nearly 10 times faster under biased condition for various concentrations of the target molecule. These results indicated that inducing ACEF can be very helpful for shortening the detection time of the biosensor.

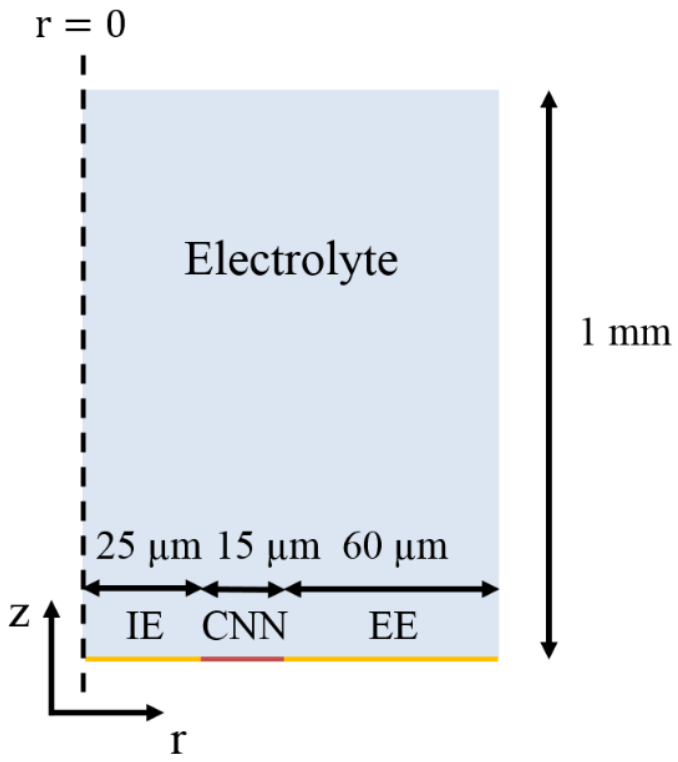

Figure 3-1 Two-dimensional cylindrical geometry defined for the COMSOL simulation [25].

Parameters	Values	Description
ε_r	78.5	Relative permittivity of the solution
σ	1 S/m	Electrical conductivity of the solution
ρ_m	$10^3 kg/m^3$	Solution mass density
C_p	$4484 \mathrm{J k} g^{-1}K^{-1}$	Heat capacity of the solution
k	$0.598 \mathrm{W} m^{-1}K^{-1}$	Thermal conductivity of the solution
η	$10^{-3} Pa \cdot s$	Viscosity of the solution
D	$0.1 \times 10^{-9} m^2/s$	Diffusion constant of the target molecule
k_{on}	$10^7 Lmol^{-1}s^{-1}$	Association rate constant
k_{off}	$3.17 \times 10^7 s^{-1}$	Dissociation rate constant
P	$10^{13} cm^{-2}$	Surface density of the probe molecule
V_{app}	0,1,3,5V	Applied bias voltage

Table 3-1 Simulation parameters [25]. For water, $\left(\frac{1}{\sigma}\right)\left(\frac{\partial \sigma}{\partial T}\right) = 0.02K^{-1}$ and $\left(\frac{1}{\varepsilon}\right)\left(\frac{\partial \varepsilon}{\partial T}\right) = -0.004K^{-1}$ [24], and the reported value of the dissociation constant between Tro6 aptamer molecules and cTnI molecules ($\mathrm{K}_d = 317\mathrm{pM}$) is considered in the simulation [19]. The association rate constant (k_{on}) and the dissociation constant (k_{off}) are assumed to satisfy the following relation, $\frac{k_{off}}{k_{on}} = K_d = 317pM$. The diffusion constant of ctnI molecules ($\mathrm{D} = 0.1 \times 10^{-9} m^2/s$) is obtained from Ref [26].

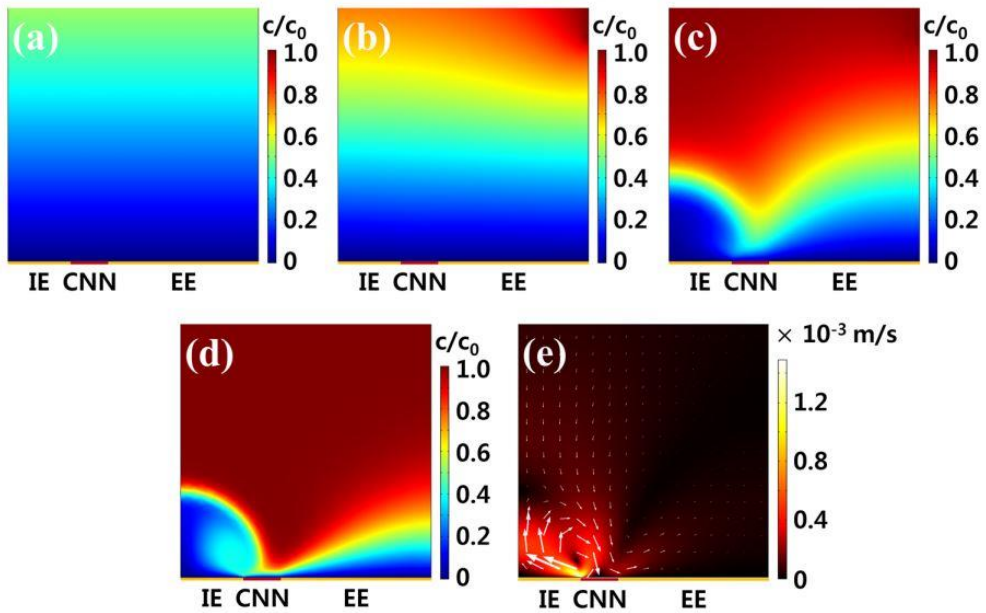

Figure 3-2 Simulation results of the binding process with an initial target concentration $C_0 = 1nM$. Target molecule concentration field for various applied AC bias amplitudes (V_{app}), (a) $V_{app} = 0V$, (b) $V_{app} = 1V$, (c) $V_{app} = 3V$, and (d) $V_{app} = 5V$ and (e) velocity field for $V_{app} = 5V$. All these plots represent the result at time = 60sec [25].

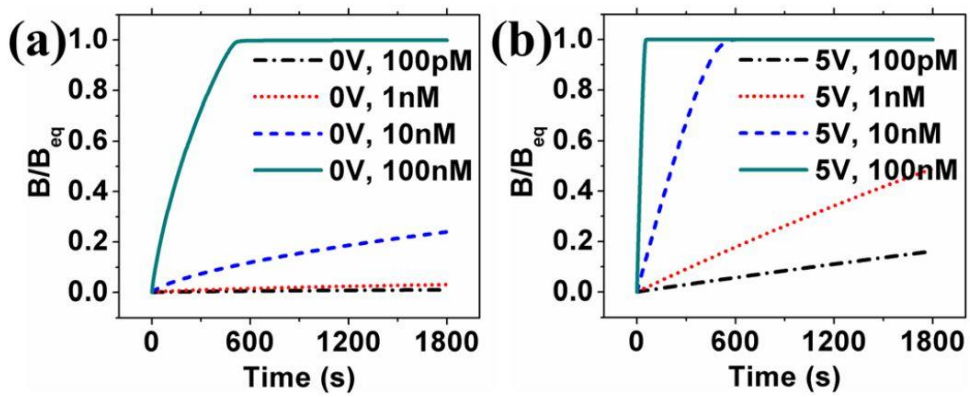

Figure 3-3 Dimensionless bound probe molecule B/B_{eq} as a function of time under (a) unbiased conditions and (b) 5V AC bias for various concentration of the target molecule [25].

Chapter 4

Electrical sensing of Troponin I (cTnI)

4.1 Introduction

In this chapter, the sensor platform is applied to detect the troponin I (cTnI), which is known as the biomarker related with the acute myocardial infarction (AMI), and analyzed. The sensor platform consists of concentric electrodes and carbon nanotube network channel region, the gold nanoparticles (GNPs) were deposited by a thermal evaporation process. The GNPs act as immobilizing sites of the probe molecules. After fabrication of the CNN-GNP-FET device, the probe molecules are immobilized on the sensor platform. The sensor structure was incubated in a phosphate-buffered saline (PBS) solution containing a 5`-thiol modified Tro6 aptamer (10μM), which is a DNA aptamer that has a high chemical affinity and specificity to cTnI, at room temperature for overnight.

The Tro6 aptamers are self-assembled on the GNPs by forming gold-thiol chemical bonds. The binding reaction between Tro6 aptamer and target protein molecule leads to the change of channel current, which is the indicator to

estimate the amount of the bound protein.

In the following sections, two distinctive electrical techniques were applied to the sensor platform. First, the pulse measurement used in the sensing event (after the binding event) and then the method of ACEF used in the binding event are explained.

4.2 Sensing event: pulse measurement at transient state

We performed a transient measurement for the sensing event, which has previously been reported [14]. The step pulse (+1V amplitude, 100μsec duty) generated by the function generator was applied to the CNN, and an inverting operational amplifier circuit was used to convert the output current to the voltage signals as shown in the figure 4-1. As well characterized, the electric field fades away beyond the "Debye screening length", which is the distance where moving charge carriers screen out the external electric field. Therefore, this Debye screening length has become one of the main disadvantage in measuring the biomolecular recognition using a FET biosensor. In the transient measurement, the channel current is measured before the ions in the electrical double layer (EDL) are redistributed, in other words, avoiding the charge screening effect. By applying a step pulse to the island electrode, the counter ions surrounding the charged target molecule are swept away by the electric

field in the extended EDL during the transient state. So the field effect of the charged target molecules on the CNN channel region can be amplified. The figure 4-2. illustrates the transient measurement after pulse bias. Because the output of step pulse includes both capacitive current and CNT channel current, we subtracted the capacitive current from the total current to get the CNT channel current as shown in the figure 4-3. The sensitivity is defined as the CNT current change after the binding event of the target antigen.

4.3 Binding event: AC electrothermal flow

We applied an AC bias (3,5 V amplitude, 1 MHz frequency) for the binding event to achieve the microstirring effect of the ACEF. A frequency of 1 MHz was selected because at lower frequencies ($\ll$1 MHz), most of the applied potential drops across the thin electric double layer at the electrode surface because the RC time constant of our platform immersed in electrolyte is approximately a few microseconds [14]. therefore, the electric field in the bulk electrolyte decreases so that the associated. Electrolysis can be avoided by the selection of a 1MHz frequency because only a small fraction of the applied potential drops across the thin electric double layer. As we verified with the simulation studies, a higher amplitude led to more effective ACEF. Although

high voltage DC bias can lead to severe electrolysis, a 1 MHz frequency allowed us to apply high amplitude bias while avoiding electrolysis because of the small potential drop across the electric double layer. However, even the degradation of the sensor platform and water electrolysis were observed at bias amplitudes above 5V. therefore, the bias amplitude of 5V or less has selected in the experiment.

4.4 Experiment results for sensing cTnI in PBS

To verify the simulation results, the first set of experiment is to detect cTnI using the sensor platform in the PBS condition.

As mentioned in the previous section, we used two distinctive techniques for the cTnI sensing. First, after the addition of the target solution, a non-uniform AC electric field is applied to induce an electric field to stir the flow field in order to improve the performance of the biosensor by accelerating the transport speed. The applied ac potential was ± 5V at 1MHz for 30min. After 30 min of binding under AC biasing, we performed a transient measurement method for sensing, which has previously been reported [14]. The step pulse (1 V amplitude, 100 μsec duty) generated by the function generator was applied to the CNN, and an inverting operational amplifier circuit was used to convert the output current to the voltage signals. We defined the sensitivity as

the ratio of the difference in channel current before and after probe–target hybridization.

The figure 4-4 illustrates the total sensing process flow for the measurement scheme.

The figure 4-5(a) and (b) show the transient measurement results after 30 min of AC bias and no bias, respectively. A clear response was obtained in the AC bias experiments for the cTnI concentrations of 100 pM~100 nM. As the target concentrations increased, the current change has increased. As the isoelectric point of cTnI is 9.87, cTnI has a positive charge in the PBS solution. Therefore, the cTnI molecule bound with the Tro6 aptamer on the GNP was expected to show a positive-gating effect on the p-type carbon nanotubes, which directly led to the decrease in the current flow through the CNN region.

Compared with the clear sensing signal obtained for the sample go through the AC bias during the binding event, inferior sensing sensitivity was observed for the sample without the AC bias after the binding event of 30 min. The sensor could only detect cTnI down to the concentrations of 100 nM and failed to detect lower concentrations of cTnI. Therefore, we concluded that the ACEF is highly effective at increasing the probe–target binding rate and, consequently, improving the detection limit of the biosensor by approximately 1–2 orders of magnitude.

We investigated the selectivity of our system, which is another important performance factor for a biosensor, by conducting control experiments using the bovine serum albumin (BSA), thrombin, and ErbB2 as the nonspecific targets. Despite the high concentrations of these non-target molecules (100 nM), the observed change in the signal was only approximately 5%, which was much smaller than the signal change obtained for the experiment with the same concentration of cTnI. These results demonstrated that the sensor could selectively detect the target molecule cTnI.

We also compared the settling time of the sensor signal under both AC bias and unbiased conditions in the 100 nM cTnI solution, as shown in the fig 4-5(d).

We obtained the transient measurements every 10 min for 90 min and plotted the average value of the 10 measurement points (100 ns) around 1us where the sensor shows a maximum signal. It has been reported that more than an hour is needed for the sensor signal to reach a steady state. In the case of our sensor platform, the sensitivity did not reach the saturation point even after 90 min of measurement in the 100 nM cTnI solution under no bias. However, under AC bias, the signal change was fast and the saturation was almost complete after 90 min of measurement. Therefore, it may be argued that the ACEF can be used to reduce the settling time of the biosensor and is effective

at improving the sensor performance.

4.5 Experiment results for sensing cTnI in Human serum

From the section 4.4, the ACEF on the AuNP decorated CNN device can significantly increase the sensitivity and specificity of the biosensor assay for detecting cTnI.

It is important for development of the biosensor devices for medical applications that the sensor device is able to accurately detect the low concentrations of biomarkers under the human serum condition.

A major challenge in the development of label-free biosensors is to differentiate the specific capture of the target of interest from the non-specific adsorption of other materials (noisy molecules) in the real serum.

The non-specific binding is caused by molecular forces between the analyte and the sensor surface. To reduce and prevent the non-specific binding, the chemical and physical methods have been suggested as follows.

First, TWEEN 20, a detergent applied to forming the blocking layer to prevent the nonspecific binding, is one of the most widely used molecules [27]. The structure of TWEEN20 consists of the two sides of different chemical properties, one with the hydrophobic and the other is the hydrophilic

characteristics. The hydrophobic side of TWEEN20 interacts with the surface of the CNT, which shows also hydrophobic property, and forms strong adsorption under irreversible chemical reaction between the hydrophobic-to-hydrophobic interactions. Therefore, after forming the blocking layer with the TWEEN20, the hydrophilic side of TWEEN20 is exposed on the CNT channel surface, where the hydrophilic surface repels the nonspecific proteins from the surface of the channel region and prevents the hydrophobic interaction.

To confirm the effect of TWEEN 20 on the CNT surface, two sample devices with and without TWEEN 20 are prepared. Figure 4-6 shows the transient measurement results after the binding event under the AC-biased condition. The signal change is more (so the sensitivity is better) for the sample with the TWEEN 20 blocking layer than the sample without TWEEN 20 blocking layer.

Second, after the binding event under the AC bias condition, a washing step was applied to remove the excessively adsorbed the non-specific molecules using deionized water. After rinsing thoroughly with deionized water, the transient measurement was performed again in the PBS buffer solution.

The biosensor platform was functionalized with the Tro6 aptamers as described above and used to detect cTnI for various concentrations in the human serum solution.

In the preparation of the biosensor platform, the channel integrated CNN-GNPs was exposed to an aqueous Tro6 aptamer solution (PBS, pH7.4) for 12hours at room temperature and then rinsed several times with the deionized water to remove nonspecific binding of unwanted molecules to the sensor platform. Then, the 1% TWEEN 20 dissolved in the PBS was injected into the test chip which was functionalized with the Tro6 aptamer.

To detect the cTnI biomarkers in the human serum solution, the AC bias similar to the method described in the section 4.4 has been applied. During the binding event, $\pm 3V$ amplitude of the voltage was applied with 1MHz frequency at the drain electrode. After the reaction for 20minutes, the transient measurement results before and after the washing steps are compared as shown in figure 4-7. In the figure, the change in current for various concentrations of cTnI (146fM~146pM) biomarkers are shown.

We compared the current change before and after washing step and found that the outstanding advantages of the washing step. The significant improvement of sensor performance has been achieved as shown in Figure 4-8. After the washing step, the quantification of cTnI was conducted by calibration curve as shown in the figure 4-8. It has shown that the four parameters logistic regression (4PL) of the graph was highly satisfactory after the washing step and it can be used for the quantitative determination of cTnI.

The developed biosensor platform demonstrated outstanding analytical performance for relatively wide dynamic range of 146fM-146pM with the detection limit of 145fM (cut off value of cTnI: 45pg/ml~1pM). In addition, the coefficient of variation (CV) on our sensor platform was observed to be about 5% which was well within the accepted clinical range of less than 10% as shown in the table 4-1.

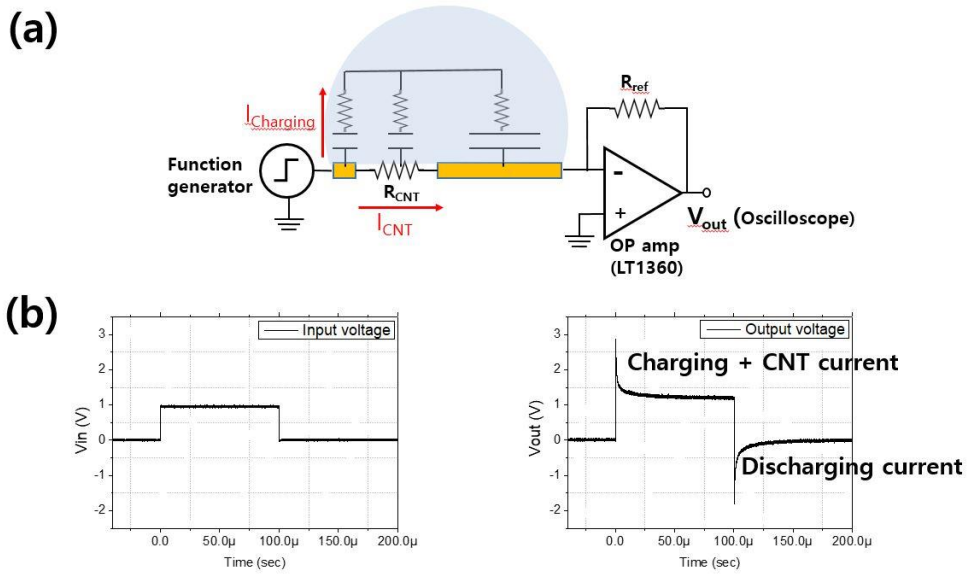

Figure 4-1 (a) The equivalent circuit diagram of the CNT network (CNN) device with the electrical measurement setup. (b) Applied pulse biasing to the drain electrode and the output voltage of the OP amplifier, which is proportional to the channel and charging current.

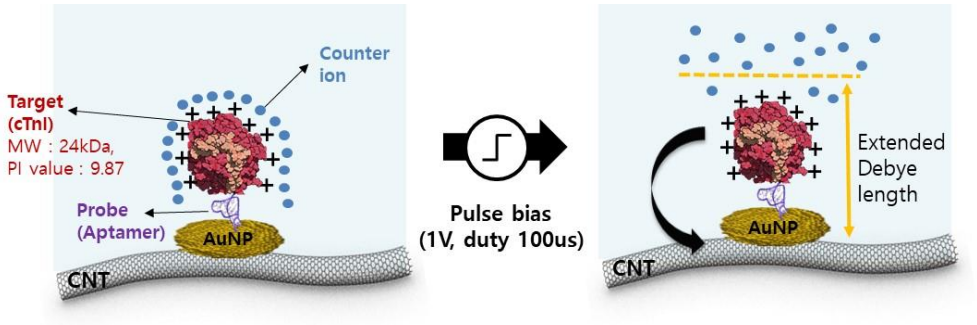

Figure 4-2 Conceptual scheme illustration of pulse measurement on transient state. There exists a space charge layer at the interface between the solution and the protein, which screens the electrostatic field induced from the charged molecule over the debyelength. After the step-pulse bias, the debyelength is extended instantaneously, the screening counter-ions around the target molecule are swept away on transient state.

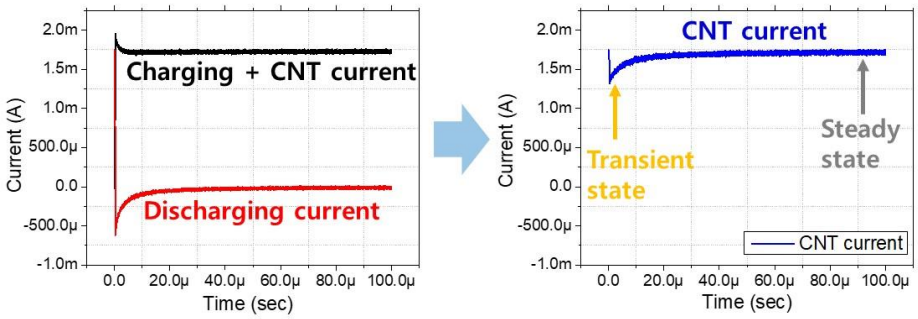

Figure 4-3 Output current from the OPAMP versus time. By subtracting discharging current from total current (Charging current + CNT current), intrinsic CNT current can be separated.

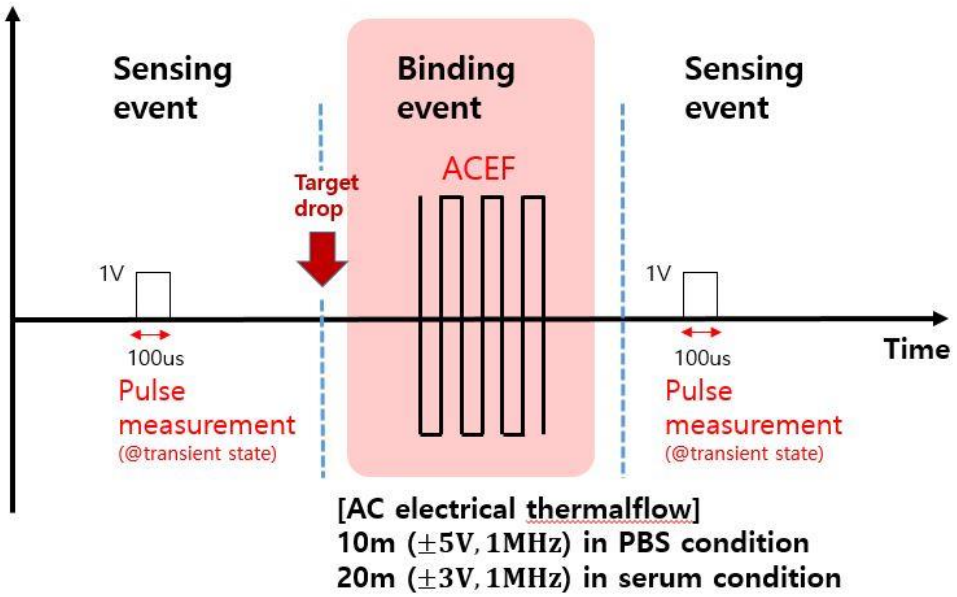

Figure 4-4 Conceptual scheme illustration of the total sensing process flow for the measurement scheme.

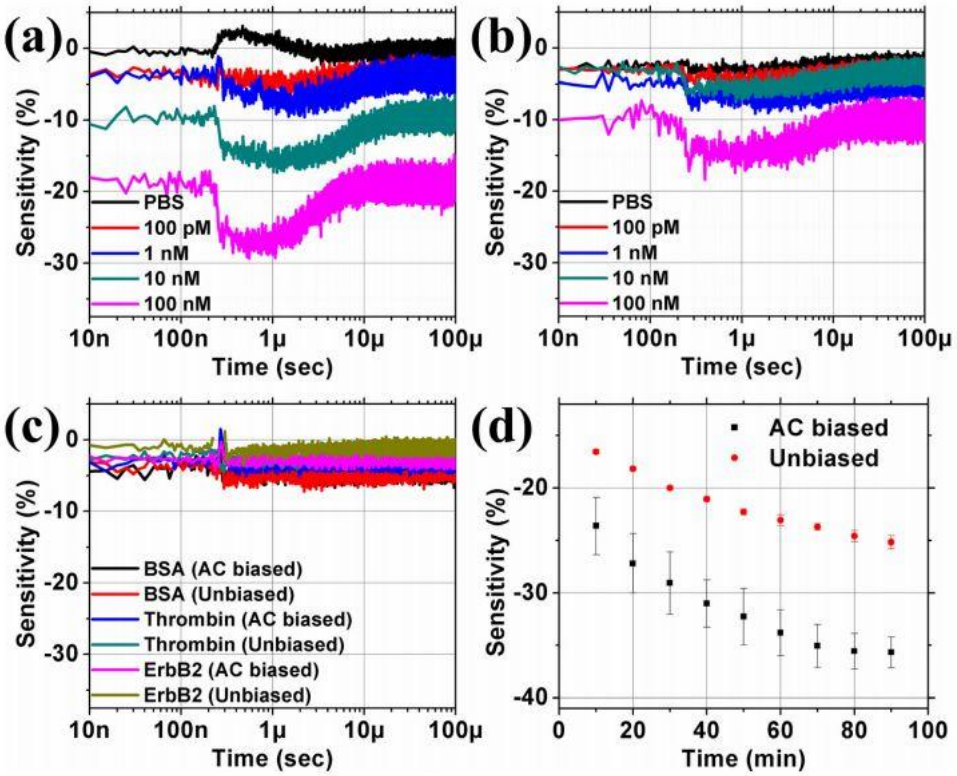

Figure 4-5 Experimental results of the transient measurement at cTnI solutions after 30min under (a) AC bias and (b) unbiased conditions. (c) Sensitivity obtained in the control experiments using non-target molecules (100nM). (d) Transient measurements data for the ctnI (100nM) sensing experiments for 90min. Each data point is an average of the measurement results from 3 independent sensors.

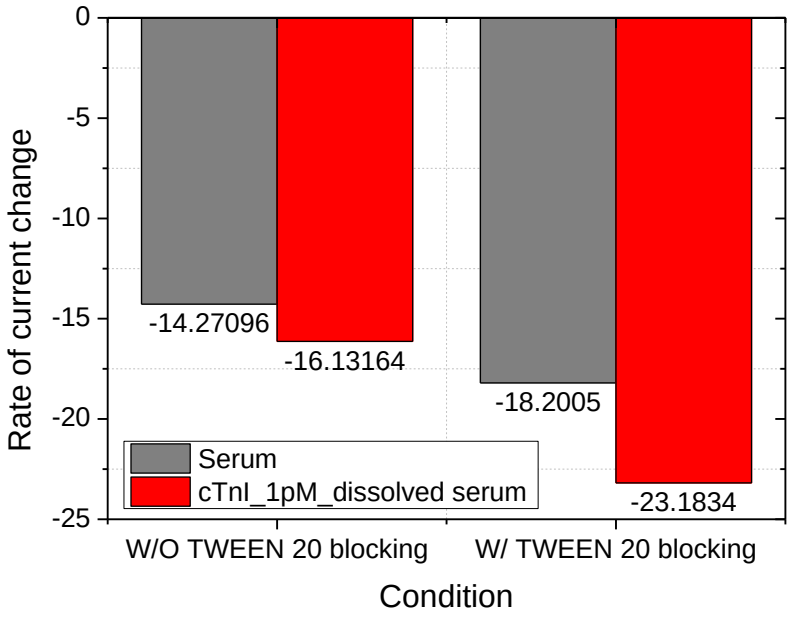

Figure 4-6 Comparison of the transient measurement results between the without TWEEN 20 and with TWEEN 20 blocking layer.

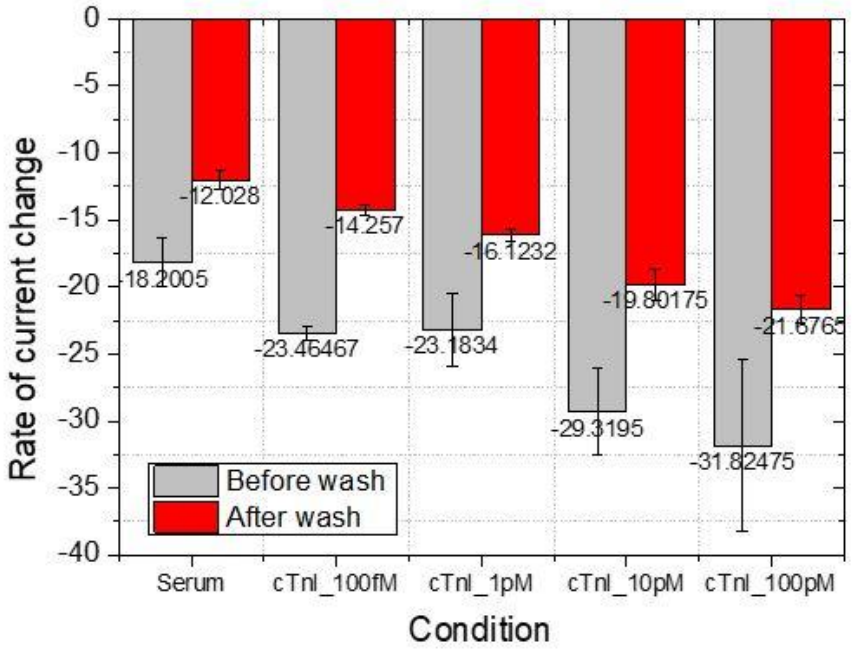

Figure 4-7 The rate of the current changes for various concentraions of the targe proteins in human serum condition.

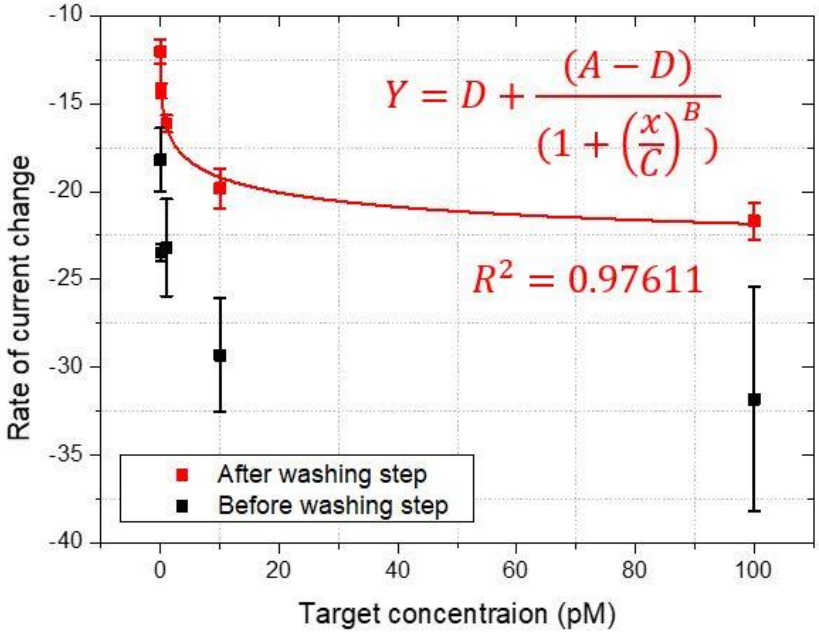

Figure 4-8 Calibration curve for the cTnI biosensor. Each point is the mean of measuremnts from 4 independent sensors. The error bars are the standard deviation.

		Serum	**cTnI 100fM**	**cTnI 1pM**	**cTnI 10pM**	**cTnI 100pM**
Before washing step	Mean	-18.2005	-23.4647	-23.1834	-29.3195	-31.8248
	Standard deriation	1.811067	0.474981	2.764919	3.232223	6.39394
	CV (%)	9.950642	2.024239	11.92629	11.02414	20.09109
After washing step	Mean	-12.028	-14.257	-16.1232	-19.8018	-21.6765
	Standard deriation	0.691137	0.411257	0.486922	1.123525	1.040562
	CV (%)	5.746068	2.8846	3.020009	5.673868	4.800414

Table 4-1 The mean value, standard deviation, and CV value of the current change are shown.

Chapter 5

Strategy for enhancement of sensor performance

5.1 Introduction

The biosensor platform operated by means of a change in the charge brought about by an interaction between the probe molecules and the target molecules. However, as seen in the previous chapter, the current change observed at a certain sampling time may not be sufficiently large to distinguish the target from the non-specific molecules. To enhance the performance of the sensor platform such as sensitivity and selectivity, the method of integration the sensing current is suggested in this chapter.

5.2 Integration of the sensing current

The inverting OPAMP is used to measure the output current of the sensor device after converting to the output voltage signals with the source (enclosing

electrode) grounded through the virtual ground as used in the previous chapter. By replacing the feedback resistance with a capacitor, the circuit performed the time integral of the total sensing current as shown in the figure 5-1.

The output current, when the pulse bias is applied, consists of both the capacitive current through the electrolyte solution and the channel current through the CNN. All these currents are integrated in time by the integrator circuit and only the channel current appear as a total charge. Notice that the charging and discharging currents are cancelled out after integration of the current.

To verify the enhancement of sensor performance, we performed the experiments for the sensing of cTnI using the current integrator. Two cases have been studied for the conditions; 1) the pristine PBS without any proteins, 2) cTnI protein dissolved in the PBS. The concentration of cTnI was 1pM(0.045ng/ml) which is the cut-off level of the AMI diagnosis condition.

5.3 The data from the integration measurement

The step pulse (1 V amplitude, 100μsec duty) generated by the function generator, which is the same condition as the sensing event, was applied to the CNN, and an integrator circuit was used to integrate of the total current.

In figure 5-2, the change of the integrated current after injection of the PBS with and without the target proteins. In case of the PBS with target, cTnI of 1pM has been dissolved in PBS. The sensitiviy is defined as the difference of the integrated current before and after binding events with the target proteins.

Compared to the transient measurement, the integrated measurement has shown almost the same sensitivity as shown in the figure 5-3.

In the previous chapter, the sensitivity of electrical sensing method has been maximized by implementation of the transient measurement. The sensitivity was plotted the average value of the CNT currnet around 1μsec where the sensor shows a maximum signal. Therefore, an attempts to improve the sensitivity of cTnI have been proposed in the transient states. We compared the case of applying the pulse once and the case of applying the pulse several times shortly (only transient states existed) during the same period. The schematic of output current according to two cases are shown in the figure 5-4. When the pulse was applied only once, both the transient state and the steady state existed. On the other hand, if short pulse is applied several times, there is only the transient state.

Pulses with long and short widths (100μsec and 1μsec) have been applied to the drain (the island electrode) by the function generator. As seen in the figure 5-5, the integrated current change according to the pulse width (100μsec and

1μsec) for the same period.

From the data after applying short pulses several times in a short time, it was confirmed that the sensitivity was improved more than the case when the pulse was applied once as shown in the figure 5-6. These results demonstrate that the integrated measurement is very effective for increasing the sensitivity compared to the transient measurement where the current is taken once for a certain fixed time.

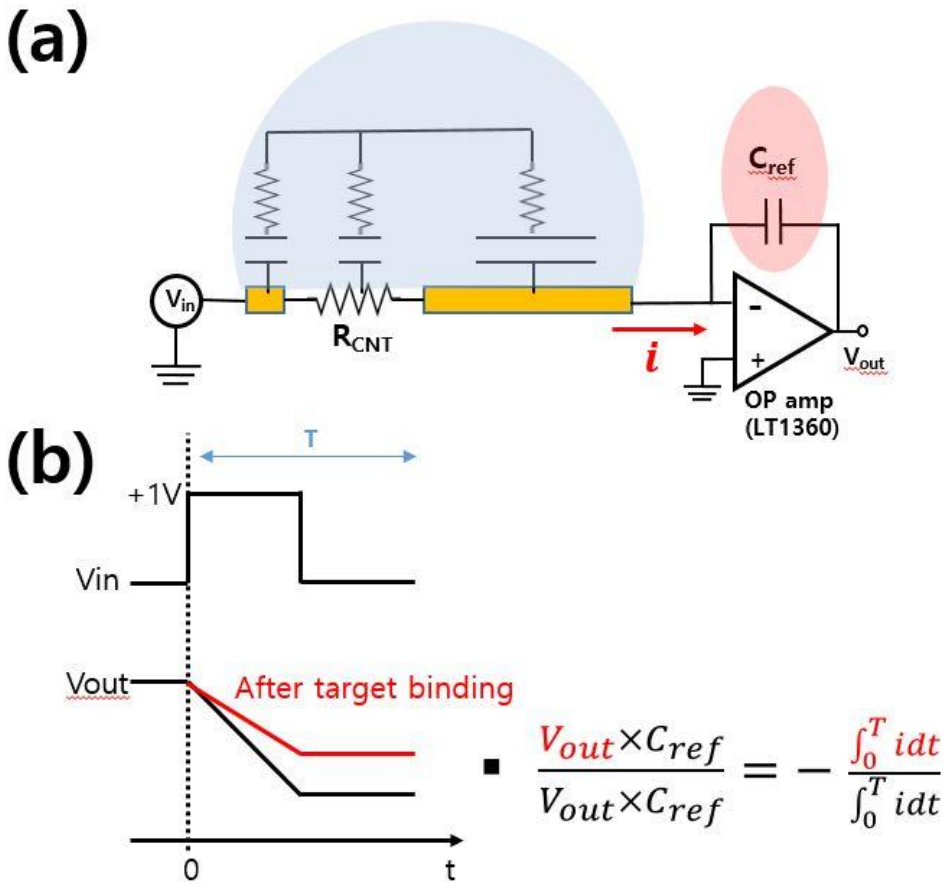

$$\blacksquare \quad \frac{V_{out} \times C_{ref}}{V_{out} \times C_{ref}} = -\frac{\int_0^T idt}{\int_0^T idt}$$

Figure 5-1 (a) The equivalent circuit diagram of the CNT network (CNN) device with the electrical integration measurement setup. (b) Applied pulse biasing to the drain electrode and the output was shown before and after injection of the target solution.

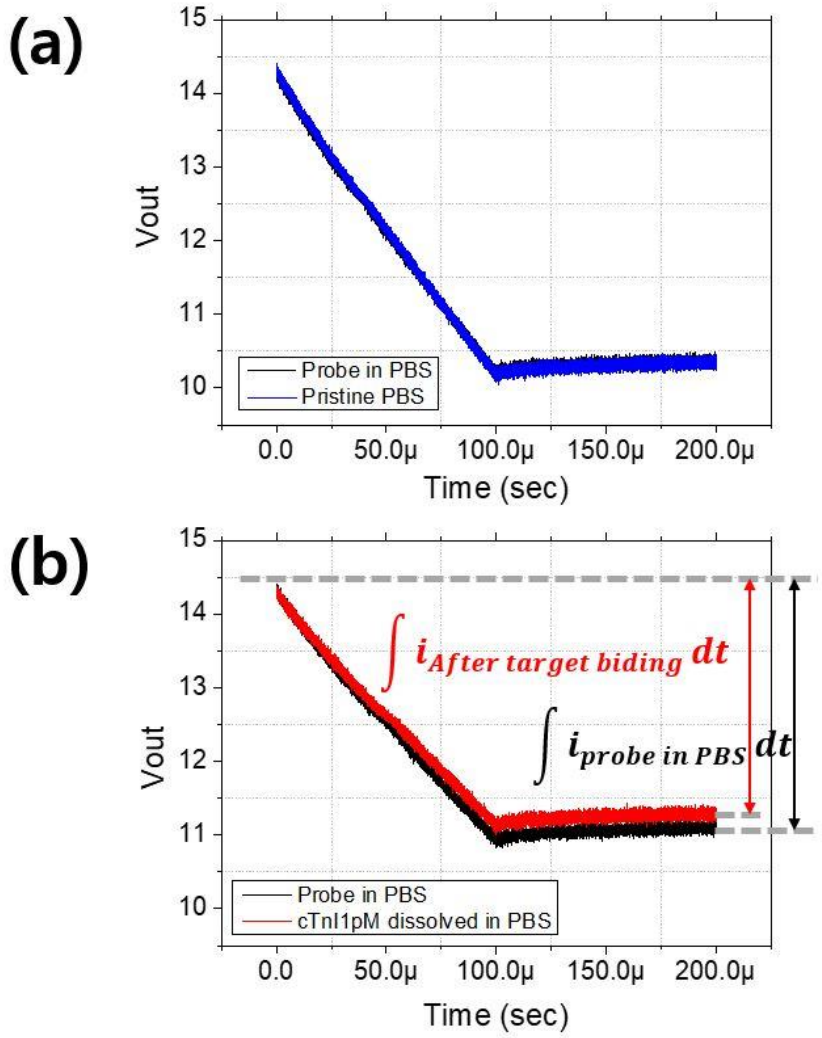

Figure 5-2 The change of integration current after injection of (a) PBS and (b) PBS with target cTnI of 1pM.

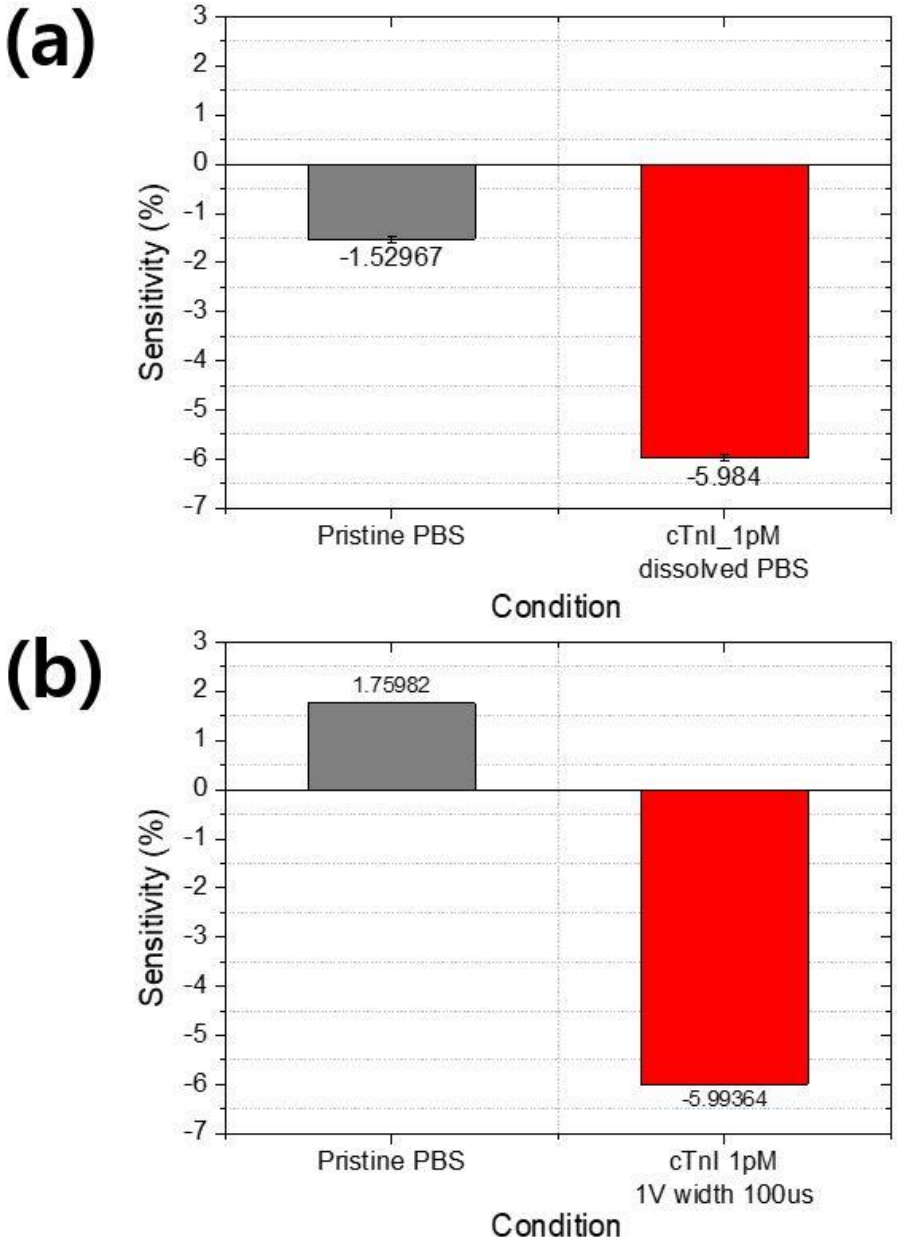

Figure 5-3 Comparison between the result of (a) transient measurement and (b) integration measurement. The sensitiviy is defined as the difference of the integrated current before and after the target reaction.

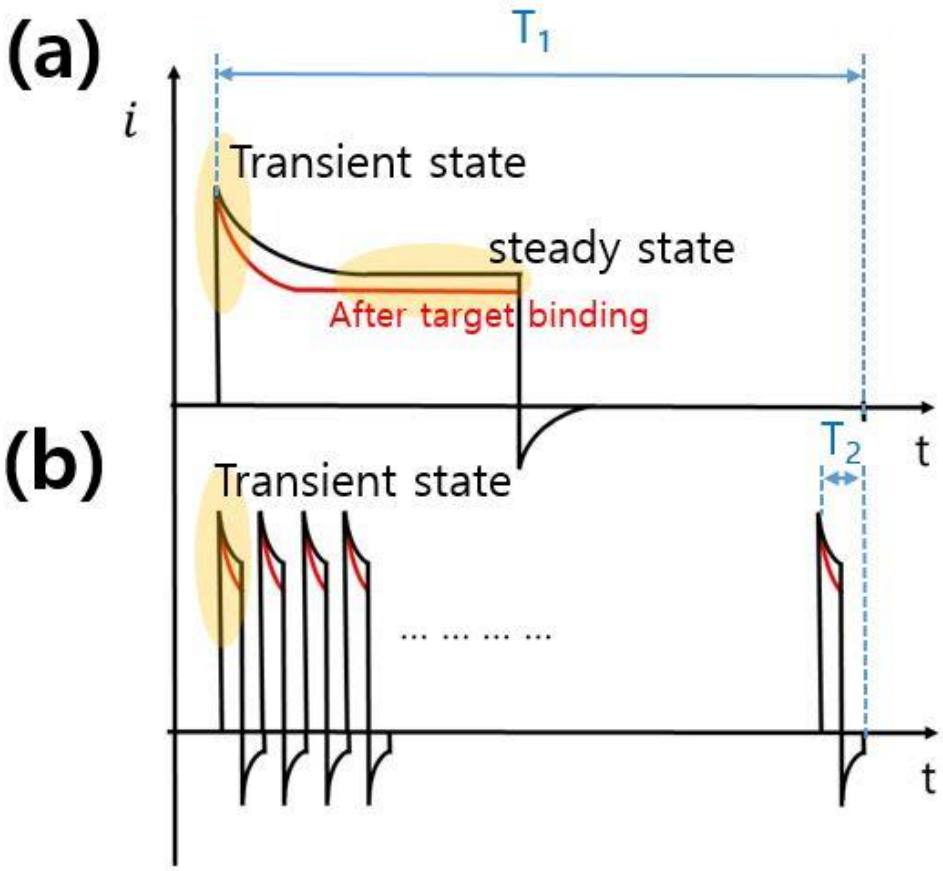

Figure 5-4. Schematic of output current . (a) When the pulse was applied only once, both the transient state and the steady state existed. (b) On the other hand, if the pulse is applied several times shortly, there is only a transient state.

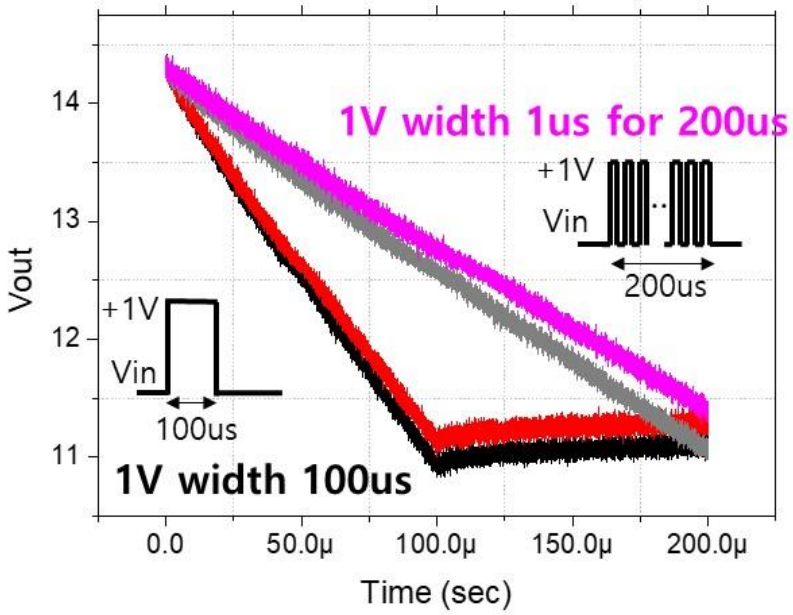

Figure 5-5 The comparison of the change of integration current between the case of applying the pulse once and the case of applying the pulse several times shortly (transient state) during the same period (200μsec).

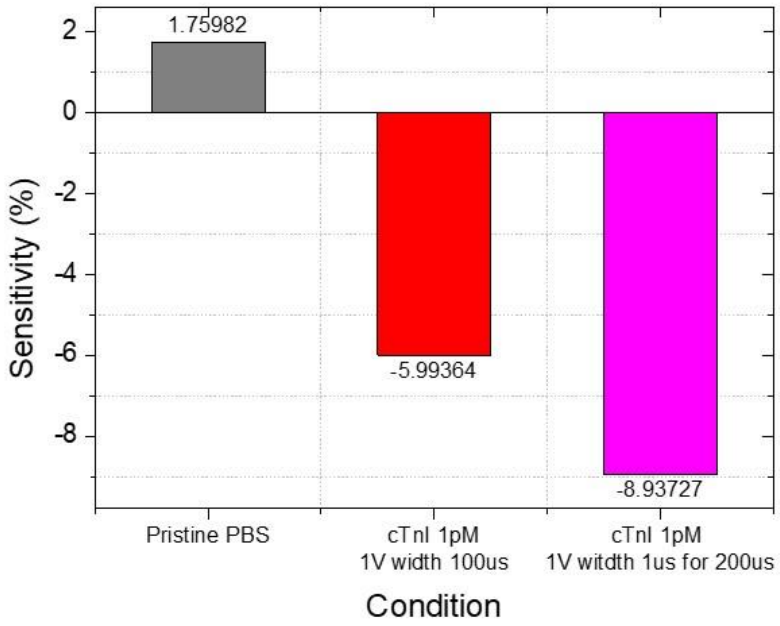

Figure 5-6 The integrated current changes for 1) pristine without target , for target samples with 2) applying the pulse once and 3) applying short pulses several times for the same period (200μsec) as in 2).

Chapter 6

Conclusion

6.1 Summary

We have developed a label-free and sensitive CNN based electrical sensor platform for the detection of cTnI which is a diagnostic biomarker for AMI.

For enhancing the sensitivity of the sensor devices, the transient measurement of the current was used to remove the Debye screening effect caused by the high ion concentration in the electrolyte solution. Also, the microstirring using ACEF method has been applied during the binding event to enhance the binding kinetics between the target and probe molecules.

The simulation results indicated that our concentric sensor platform is suitable to apply the ACEF method to concentrate the target molecules toward the sensing region. The experimental results showed that enhanced detection of the cTnI was achieved using the ACEF method comparing with the data without electrical bias during the binding event. To reduce and prevent the non-specific binding, the chemical and physical methods were introduced. First, TWEEN 20 is used as the detergent to form the blocking layer to prevent the

nonspecific binding. Second, in addition to applying the ACEF, a washing step using deionized water was applied to remove excess adsorbed the non-specific molecules. The developed biosensor platform demonstrated outstanding analytical performance with a relatively dynamic range of 146fM-146pM and the detection limit of 145fM in the human serum condition. The coefficient of variation (CV) on our sensor platform was observed to be about 5%, which is well within the accepted clinical range of less than 10%.

To enhance the performance of the sensor platform, the method of integration current rather than onetime current measurement was suggested. When the short pulse train was applied giving only the transient state during the current measurement, it was confirmed that the sensitivity was improved quite appreciably.

6.2 Future work

In order to meet the need of early detection of disease, our group has developed the CNT based sensor with two electrodes system. It has been shown that our sensor platform meets the need by providing,

- Label free detection of the DNA, protein molecules as the biomarker,
- Enhancement of the binding event between the target and probe molecules

by applying the ACEF method,

- Enhancement of the sensitivity by applying the electrical pulses (both the one time measurement of the sensor current and current integration methods),

- And other chemical and physical means to remove the nonselective molecules bound to the channel.

This dissertation is on the application of our sensor platform to detect the cTnI molecules as the biomarker of the cardiac disease such as AMI with the aptmer molecules as the probe. Satisfactory results for the sensitivity, LOD and CV data have been obtained.

In order for the sensor platform to be the practical real time monitor tool for various diseases including AMI, the following works have to be done before going through the FDA approval;

- Miniaturization of the electrical circuits to provide both ACEF and pulse train for both the binding event and sensing current.

- A simple and reliable well structure integrated to the sensor devices to accept the small quantity of human blood sample as small as 10uL.

- A simple and reliable filtering method equipped on the well structure, thereby red blood cells, clotting elements in the blood are filtered out and serum with the biomarker molecules is applied to the channel region of the sensor devices.

References

[1] Z. Altintas, W. M. Fakanya, and I. E. Tothill, “Cardiovascular disease detection using bio-sensing techniques,” *Talanta*, vol. 128, pp. 177–186, 2014.

[2] A. Qureshi, Y. Gurbuz, and J. H. Niazi, “Biosensors for cardiac biomarkers detection: A review,” *Sensors Actuators, B Chem.*, vol. 171–172, pp. 62–76, 2012.

[3] K. Thygesen *et al.*, “Third universal definition of myocardial infarction,” *Eur. Heart J.*, vol. 33, no. 20, pp. 2551–2567, 2012.

[4] J. H. Nichols *et al.*, “Executive summary. The National Academy of Clinical Biochemistry Laboratory Medicine Practice Guideline: Evidence-based practice for point-of-care testing,” *Clin. Chim. Acta*, vol. 379, no. 1–2, pp. 14–28, 2007.

[5] J. J. Gooding, “Biosensor technology for detecting biological warfare agents: Recent progress and future trends,” *Anal. Chim. Acta*, vol. 559, no. 2, pp. 137–151, 2006.

[6] P. E. Sheehan and L. J. Whitman, “Detection limits for nanoscale biosensors,” *Nano Lett.*, vol. 5, no. 4, pp. 803–807, 2005.

[7] P. R. Nair and M. A. Alam, “Performance limits of nanobiosensors,” *Appl. Phys. Lett.*, vol. 88, no. 23, pp. 98–101, 2006.

[8] a Ramos, H. Morgan, N. G. Green, and A. Castellanos, “Ac electrokinetics: a review of forces in microelectrode structures,” *J. Phys. D. Appl. Phys.*, vol. 31, no. 18, pp. 2338–2353, 1999.

[9] M. Sigurdson, D. Wang, and C. D. Meinhart, “Electrothermal stirring for heterogeneous immunoassays.,” *Lab Chip*, vol. 5, no. 12, pp. 1366–1373, 2005.

[10] J. H. Cheon *et al.*, “Electrical characteristics of the concentric-shape

carbon nanotube network device in pH buffer solution," *IEEE Trans. Electron Devices*, vol. 57, no. 10, pp. 2684–2689, 2010.

[11] S. M. Seo *et al.*, "Statistical property of the effect of Au nanoparticle decoration on the carbon nanotube network," *Appl. Phys. Lett.*, vol. 98, no. 14, pp. 1–4, 2011.

[12] J. W. Ko *et al.*, "Multi-order dynamic range DNA sensor using a gold decorated SWCNT random network," *ACS Nano*, vol. 5, no. 6, pp. 4365–4372, 2011.

[13] D. W. Kim *et al.*, "Self-gating effects in carbon nanotube network based liquid gate field effect transistors," *Appl. Phys. Lett.*, vol. 93, no. 24, pp. 1–4, 2008.

[14] J.-M. Woo, S. H. Kim, H. Chun, S. J. Kim, J. Ahn, and Y. J. Park, "Modulation of molecular hybridization and charge screening in a carbon nanotube network channel using the electrical pulse method.," *Lab Chip*, vol. 13, no. 18, pp. 3755–63, 2013.

[15] S. H. Kim, J. M. Woo, S. Choi, and Y. J. Park, "Electrical passivation of nonselective bio molecules in carbon nanotubes: Effect of pulse train in serum," *Appl. Phys. Lett.*, vol. 106, no. 26, 2015.

[16] E. Y. Jang, T. J. Kang, H. W. Im, D. W. Kim, and Y. H. Kim, "Single-walled carbon-nanotube networks on large-area glass substrate by the dip-coating method," *Small*, vol. 4, no. 12, pp. 2255–2261, 2008.

[17] A. Star, V. Joshi, S. Skarupo, D. Thomas, and J. C. P. Gabriel, "Gas sensor array based on metal-decorated carbon nanotubes," *J. Phys. Chem. B*, vol. 110, no. 42, pp. 21014–21020, 2006.

[18] M. Muratsugu *et al.*, "Quartz Crystal Microbalance for the Detection of Microgram Quantities of Human Serum Albumin: Relationship Between the Frequency Change and the Mass of Protein Adsorbed," *Anal. Chem.*, vol. 65, no. 20, pp. 2933–2937, 1993.

[19] H. Jo *et al.*, "Electrochemical Aptasensor of Cardiac Troponin I for the Early Diagnosis of Acute Myocardial Infarction," *Anal. Chem.*, vol. 87, no. 19, pp. 9869–9875, Oct. 2015.

[20] H. Yang, V. N. Luk, M. Abelgawad, I. Barbulovic-nad, and A. R. Wheeler, “Article A World-to-Chip Interface for Digital Microfluidics A World-to-Chip Interface for Digital Microfluidics,” *Anal. Chem.*, vol. 81, no. December 2008, pp. 1061–1067, 2009.

[21] P. K. Wong, T.-H. Wang, J. H. Deval, and C.-M. Ho, “Electrokinetics in Micro Devices for Biotechnology Applications,” *IEEE/ASME Trans. Mechatronics*, vol. 9, no. 2, pp. 366–376, Jun. 2004.

[22] J. Oh, R. Hart, J. Capurro, and H. M. Noh, “Comprehensive analysis of particle motion under non-uniform AC electric fields in a microchannel.,” *Lab Chip*, vol. 9, no. 1, pp. 62–78, 2009.

[23] A. Salari and M. Thompson, “Recent advances in AC electrokinetic sample enrichment techniques for biosensor development,” *Sensors Actuators, B Chem.*, vol. 255, pp. 3601–3615, 2018.

[24] D. R. Lide, “CRC Handbook of Chemistry and Physics,” *eBook*, p. 3485, 2003.

[25] W. C. Lee, H. Lee, J. Lim, and Y. J. Park, “An effective electrical sensing scheme using AC electrothermal flow on a biosensor platform based on a carbon nanotube network,” *Appl. Phys. Lett.*, vol. 109, no. 22, p. 223701, 2016.

[26] T. Jacroux, D. Bottenus, B. Rieck, C. F. Ivory, and W. J. I. Dong, “Cationic isotachophoresis separation of the biomarker cardiac troponin I from a high-abundance contaminant, serum albumin,” *Electrophoresis*, vol. 35, no. 14, pp. 2029–2038, 2014.

[27] R. J. Chen *et al.*, “Noncovalent functionalization of carbon nanotubes for highly specific electronic biosensors.,” *Proc. Natl. Acad. Sci. U. S. A.*, vol. 100, no. 9, pp. 4984–4989, 2003.

초록

급성 심근 경색의 진단에서 바이오마커를 빨리 검출하는 것이 중요한 지표가 되고 있고, 바이오마커 중 트로포닌이라는 물질이 현재 가장 각광받고 있는 진단 지표 바이오마커이다.

나노 금 입자로 증착된 카본 나노 튜브를 채널로 가지는 이 전극 전기 바이오칩을 금성 심근 경색 바이오마커인 ‘트로포닌 I’를 측정하는 바이오칩을 개발하였다. 바이오 마커에 친화도가 좋은 프로브 물질로 ‘압타머’를 사용하였다.

본 논문의 기여는 크게 세 가지로 정리할 수 있다.

첫 번째, 압타머-트로포닌 I 결합을 근거로한 전기 바이오칩 구현. (본 연구실에서 개발한 C-chip에서 첫 시도와 친화도를 개선하기 위해서 ACEF 방법을 이 단자 전극에 적용한 첫 시도)

두 번째, 압타머-트로포닌 I 결합 이 후, 민감도를 개선하기 위해서 펄스 방법을 시도하고, 이를 적분 방법으로 개선하려는 첫 시도해 보았다.

세 번째, 실제 환자에게 적용하기 위해서 세럼 환경에서 시도해 보았다.

이상 시도로, 본 C-chip이 심근경색의 빠른 현장검사 응용에 적합함을 보인 논문이다. 실험 결과로 C-chip에서의 검출한계는 세럼 환경에서 4.5pg/ml 이하로 컷오프 값인 45pg/ml 보다 낮은 농도에서 검출 가능함을 확인 하였다.

주요어 : 탄소나노튜브, 금 나노입자, 압타머, 단백질 센서, ACEF, 급성 심근 경색

학번 : 2012-20848